Mol. Cryst. Liq. Cryst., Vol. 455, pp. 287–294, 2006

ISSN: 1542-1406 print/1563-5287 online
DOI: 10.1080/15421400600698758

Taylor & Francis
Taylor & Francis Group

Trigonal Anisotropy in Graphite and Carbon Nanotubes

R. Saito
J. Jiang
A. Gruneis
K. Sato
Y. Oyama
Department of Physics, Tohoku University and CREST JST, Aoba, Japan

Ge. G. Samsonidze
S. G. Chou
G. Dresselhaus
M. S. Dresselhaus
Massachusetts Institute of Technology, Cambridge, Massachusetts, USA

L. G. Cancado
C. Fantini
A. Jorio
M. A. Pimenta
Departmento de Fisica, Universidade Federal de Minas Gerais, Bero Horizonte, Brazil

We discuss here how the trigonal warping effect of the electronic structure is relevant to optical processes in graphite and carbon nanotubes. The electron-photon, electron-phonon, and elastic scattering matrix elements have a common factor of the coefficients of Bloch wave funtions of the A and B atoms in the graphite unit cell. Because of the three fold symmetry around the Fermi energy point (the K or K′ point), the matrix elements show a trigonal anisotropy which can be observed in both resonance Raman and photoluminescence spectroscopy. This anisotropy is essential for understanding the chirality dependence of the Raman intensity and the optical response of single wall carbon nanotubes.

RS acknowledges a Grant-in-Aid (No. 16076201) from the Ministry of Education, Japan. MIT authors acknowledge support under NSF Grants DMR 04-05538 and INT 00-00408, and the Dupont-MIT alliance. UFMG authors acknowledge financial support from CNPq-Brazil.

Address correspondence to R. Saito, Department of Physics, Tohoku University and CREST JST, Aoba, Sendai 980-8578, Japan. E-mail: rsaito@phys.tohoku.ac.jp

Keywords: carbon nanotubes; electron-phonon interaction; electron-photon interaction; graphite; optical response; resonance Raman spectroscopy; trigonal warping

INTRODUCTION

Graphite has a unique electronic structure for the valence electrons in which a π electron of a carbon atom forms the valence and conduction energy bands [1]. Two dimensional graphite does not have an energy gap at the Fermi energy and the two energy bands touch each other at the zone boundary symmetry points called the K and K' points in the hexagonal Brillouin zone. Such an energy degeneracy at the zone boundary would be unstable in low dimensional materials by opening an energy gap with a $2k_F$ perturbation such as a charge density wave. However in the case of graphite, the symmetry between the two inequivalent carbon atoms, A and B, in the unit cell of graphite requires doubly degenerate energy eigenvalues which appear at the Fermi energy, E_F and thus the energy gap does not open and a linear energy dispersion of the electronic energy bands appear at E_F. Such a special situation can be seen only in graphite and single wall carbon nanotubes (SWNTs). Physical properties of graphite depend on this special electronic structure combined with the phonon structure of the sp^2 hybridized σ bonds between carbon atoms. Even though we adopted a standard formalism for basic optical processes such as optical absorption or electron-phonon interaction, the calculated results are usually anisotropic and exotic. So far we have developed computer programs for many physical matrix elements based on the tight-binding method for the π energy bands for explaining the optical absorption [2], Raman spectra [3], and photoluminescence spectra [4]. However, we did not previously consider the origin of the anisotropy of the physical properties of graphite and SWNTs in a unified view. In this paper, starting from the simple tight binding calculation, we will show the origin of the trigonal anisotropy of the physical properties of graphite and the chirality dependence of the physical properties of carbon nanotubes. Then we discuss the optical response of carbon nanotubes.

TIGHT BINDING METHODS FOR GRAPHITE AND CARBON NANOTUBES

The tight binding wave functions for the valence and conduction energy bands for graphite and carbon nanotubes $\Psi^j(k,r), (j = v,c)$ are given by the linear combination of Bloch wave functions of the A

and B atoms in the unit cell.

$$\Psi^j(k,r) = \sum_{i=A,B} C_i^j(k)\Phi_i(k,r), \quad (j = v,c), \tag{1}$$

in which $C_i^j(k)$ is the coefficient of the Bloch wave functions, and the Bloch wave function $\Phi_i(k,r)$ is given by a linear combination of atomic orbitals,

$$\Phi_i(k,r) = \frac{1}{\sqrt{N_u}} \sum_R e^{ikR} \varphi_i(r-R). \tag{2}$$

Here N_u and R are the number and position of the unit cell and $\varphi_i(r-R)$ is the atomic wavefunction of the $2p_z$ orbital of a carbon atom. In the case of a SWNT, we adopted 2s, $2p_x$, $2p_y$ orbitals, too, in the extended tight binding calculation in which the curvature effect is included by the Slater-Koster scheme [5].

The optical processes appearing in the photoluminescence (PL) and Raman spectra consist of five basic processes, as shown in Figure 1; (a) optical absorption, (b) optical emission, (c) phonon absorption, (d) phonon emission, and (e) elastic scattering by a defect. In the phonon absorption or emission processes, energy and momentum conservation rule selects the momentum $\boldsymbol{q}$ and the energy $\hbar\omega$ of a phonon. In the case of a SWNT, there are two carbon atoms in the unit cell of graphite, and thus we have six phonon dispersions which are zone-folded into one dimensional phonon branches. For each phonon dispersion of a SWNT, we have energy-momentum conserved $\boldsymbol{q}$ values for forward and backward scattering. Here the forward (backward) scattering denotes that the group velocity of an electron, which is the slope of the energy dispersion of the electron, is unchanged (changed) as is shown in Figure 2. Moreover, since there are two Fermi surfaces around the K and K′ points in the Brillouin zone, there are so called intra-valley and inter-valley scattering processes which connect the $\boldsymbol{k}$ and $\boldsymbol{k}+\boldsymbol{q}$ states from K to K (K′ to K′) and K to K′ (K′ to K), respectively. For an initial $\boldsymbol{k}$ state, there are $6 \times 2 \times 2 = 24$ possible $\boldsymbol{k}+\boldsymbol{q}$

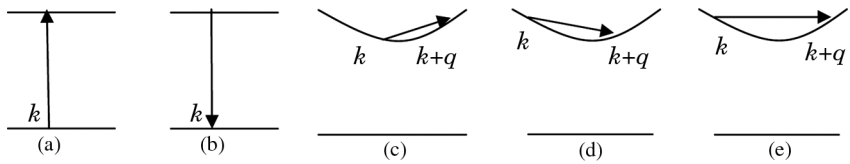

FIGURE 1 Basic optical processes: (a) optical absorption, (b) optical emission, (c) phonon absorption, (d) phonon emission, (e) elastic scattering by a defect.

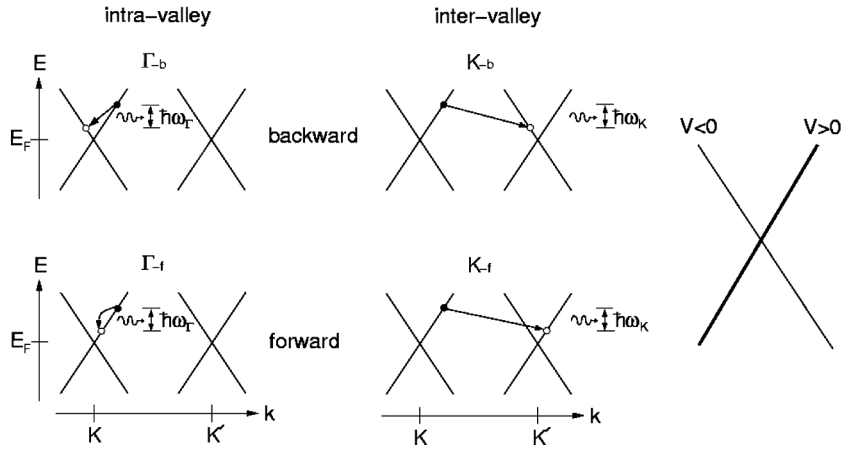

FIGURE 2 Four possible phonon emission processes for a given phonon mode. Intra-valley (left) and inter-valley (right) scattering processes correspond to the scattering from K to K and from K to K′, respectively. Backward (up) and forward (down) scattering correspond to the scattering with the opposite and the same velocity, respectively. In the right figure, we show the electronic energy band of two dimensional graphite around the K (or K′) point in which thick and thin lines denote the linear energy dispersion with positive and negative group velocity, respectively.

states for inelastic scattering for phonon absorption (emission) processes. Here we did not consider the fact that the final state is an occupied electronic state. In the case of elastic scattering, since there is no intra-valley, forward scattring, 3 possible $\boldsymbol{k}+\boldsymbol{q}$ states are expected.

The optical matrix element for an electron at $\boldsymbol{k}$ are given within the dipole approximation by

$$M_{\text{opt}}(\boldsymbol{k}) = \mathbf{P} \cdot \left\langle \Psi^{\text{C}}(\boldsymbol{k}) | \nabla | \Psi^{\text{V}}(\boldsymbol{k}) \right\rangle, \tag{3}$$

in which the $\mathbf{P}$ is the polarization vector of light. The electron-phonon matrix elements for an electron from $\boldsymbol{k}$ to $\boldsymbol{k}+\boldsymbol{q}$ for a phonon mode with wave vector $\boldsymbol{q}$ is calculated by the deformation potential approximation,

$$M_{\text{el-ph}}(\boldsymbol{k}+\boldsymbol{q}, \boldsymbol{k}) = \mathbf{A} \cdot \left\langle \Psi^{\text{C}}(\boldsymbol{k}+\boldsymbol{q}) | \nabla V | \Psi^{\text{C}}(\boldsymbol{k}) \right\rangle, \tag{4}$$

in which $\mathbf{A}$ is the amplitude vector of a phonon mode. These matrix elements have a similar form of an inner product of two vectors in which one of the two is the outer field $\mathbf{P}$ (or the phonon amplitude $\mathbf{A}$) and the other is the vector of the electronic properties as a linear response. On the other hand, the elastic scattering matrix elements

for a defect potential V is proportional to a scalar variable $\langle \Psi^{C}(\boldsymbol{k}+\boldsymbol{q})|V|\Psi^{C}(\boldsymbol{k})\rangle$. The calculation of the matrix elements is done by expanding the wavefunction to the atomic orbitals using Eqs. (1) and (2). The anisotropic behavior of graphite and carbon nanotubes is described by the coefficient $C_i^j(\boldsymbol{k})$ in Eq. (1) which is either a constant or a complex function of $f(\boldsymbol{k}) \equiv \sum_{i=1}^{3} \exp(i\boldsymbol{k}\boldsymbol{R_i})$. Here $\boldsymbol{R_i}$ $(i = 1, 2, 3)$ are three vectors of the nearest neighbor carbon sites. The function $f(\boldsymbol{k})$ has a zero value at the K (or K′) points and near the K (K′) point, $f(\boldsymbol{k})$ is a linear function of k_x and k_y. As a result, all optical properties are purely anisotropic around the K and K′ points and display the three-fold symmetry of the k space around the K and K′ points. In the case of carbon nanotubes, this anisotropy is relevant to the chirality dependence of the optical response since that the properties are relevant to the position of the van Hove singular k points. Hereafter, we show the calculated results of the optical absorption matrix elements and selection rules for electron-phonon scattering processes. The results are closely related to the chirality dependence of the optical properties for SWNTs.

RESULTS AND DISCUSSION

In Figure 3, we plot (a) the direction and (b) the absolute value (oscillator strength) of the dipole vector $\langle \Psi^{C}(\boldsymbol{k})|\nabla|\Psi^{V}(\boldsymbol{k}')\rangle$ of graphite in the

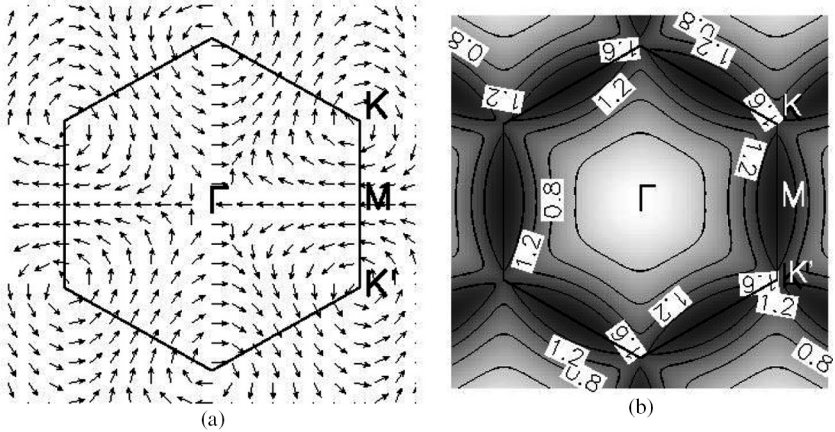

FIGURE 3 (a) The direction and (b) the absolute value of the dipole vector $\langle \Psi^{C}(\mathbf{k})|\nabla|\Psi^{V}(\mathbf{k}')\rangle$ of graphite in the two dimensional Brillouin zone. The values in (b) are shown in the units of the atomic dipole matrix elements for the nearest neighbor carbon pair [6].

two dimensional Brillouin zone [6]. The dipole vectors rotate clockwise and counter-clockwise around the K and K′ points, respectively. Since the equi-energy contour lines for the electronic energy dispersion are approximated by circles around the K and K′ points, we can expect a $\boldsymbol{k}$ dependence of the optical absorption for a given polarization vector $\mathbf{P}$. In particular, when $\mathbf{P}$ is perpendicular to the dipole vector at a $\boldsymbol{k}$ point, we expect no optical absorption (the node position) [2,7], and this effect can be observed in nano-graphite system [8]. When we see the absolute value of the dipole vector, the direction from K to the three nearest M points gives larger matrix elements (dark area) than that for the direction from K to Γ point. When the van Hove singular point is close to the K-M line, the corresponding optical transition becomes strong. This is a reason why the armchair and type I ($\mathrm{mod}(2n+m,3) = 1$ for (n,m) SWNT) semiconductor SWNTs has relatively larger values for the dipole vectors for the second van Hove singularity energy than zigzag, and type II semiconductor SWNTs. It is pointed out again that the strongly anisotropic behavior of the matrix elements is due to the coefficient of the Bloch functions.

We can not make a similar plot to Figure 3 for electron-phonon matrix elements since there are initial k and final k' states. For a given initial k state, we can plot the possible final states for each phonon mode with the wave vector q, which we found to have an anisotropy around the K or K′ points. In this case, the relative directions of the deformation vector and the phonon vibration are important, which gives a selection rule for the phonon modes in the inelastic scattering process. For example in (10,10) nanotubes, we calculated the averaged electron-phonon coupling constant for initial states at the energy 0.25 eV above the Fermi energy [9] which is listed in Table 1.

For the intra-valley electron-phonon scattering, the radial breathing mode (RBM) and the in-plane tangential optic phonon mode (iTO) have non-zero matrix elements for forwarding scattering while the twisting (TW) phonon mode, out-of-plane tangential optic phonon mode (oTO), and the longitudinal optic phonon mode (LO) have non-zero matrix elements for backward scattering. The RBM, iTO and LO phonon modes

TABLE 1 Non-zero Electron-phonon Matrix Elements for Each Type of Inelastic Scattering Calculated for an (10,10) Armchair Nanotube at the Energy 0.25 eV above the Fermi Energy

	Forward scattering	Backward scattering
Intra-valley scattering	RBM, iTO	TW, oTO, LO
Inter-valley scattering	$E_2(1)$, $E_1(1)$	$E_2(2)$, $E_1(2)$, A_1

correspond to the RBM, G− and G+ Raman modes, respectively. The TW and oTO phonon modes can be seen in Raman spectroscopy only in second-order processes. The longitudinal acoustic (LA) phonon mode does not contribute the electron-phonon matrix element either for forward or backward scattering. Though the oTO phonon mode has no electron-phonon matrix elements in graphite, the oTO electron-phonon matrix element exists for a SWNT due to the curvature effect of the SWNT which is proportional to the inverse square of the diameter.

For inter-valley electron-phonon scattering, the phonon modes around the K (K′) point are relevant. At the K (K′) point, two E modes appear; two longitudinal phonon modes E_1 (LA and LO branches) and two out-of-plane phonon modes E_2 (oTA and oTO branches). The remaining two tangential phonon branches give two, non-degenerate A modes (A_1 iTO, A_2 TW branches). The electron-phonon matrix elements have a non-zero forward scattering matrix element for one of two representations for the E_1 and E_2 mode ($E_1(1)$ and $E_2(1)$), and also a non-zero, backward scattering for the $E_1(2)$, $E_2(2)$, and A_1 modes. The symmetry selection rule for the electron-phonon matrix elements are closely related to the appearance of a chirality dependence of the relative intensity of the G−/G+ Raman intensity and of the RBM intensity. For example, the calculated results for the RBM and TO (G− band) Raman feature show a larger chiral angle dependence than the diameter dependence in which the same $n-m$ value for (n,m) SWNTs gives similar intensity values (family pattern). On the other hand, the LO (G+) band shows no significant chirality dependence. Thus the relative G−/G+ Raman intensity has maximum (minimum) values for armchair (zigzag) nanotubes which is consistent with the experimental observations of single nanotube Raman spectroscopy [10,11]. As for the RBM intensity, a zigzag nanotube gives a larger intensity than an armchair nanotube, and the RBM intensity decreases with increasing the diameter for a given chiral angle. Since the electron-phonon calculation needs to be calculated for many k and k′ states for (n,m) SWNTs, a detailed report of the Raman intensity and PL intensity will be reported elsewhere [9].

In summary, we show that the PL and Raman intensity in graphite has a strong k dependence which is reflected in the chirality dependence of the intensity in single wall carbon nanotubes. The electron-photon and electron-phonon interactions give a similar functional form within the extended tight binding scheme and the anisotropy of the coefficient of the Bloch wave functions in the valence and conduction energy bands play a crucial role in the chirality dependence of the matrix elements, and in the physical processes depending on these matrix elements.

REFERENCES

[1] Saito, R., Dresselhaus, G., & Dresselhaus, M. S. (1998). *Physical Properties of Carbon Nanotubes*, Imperial College Press, London, UK.
[2] Jiang, J., Saito, R., Grueneis, A., Dresselhaus, G., & Dresselhaus, M. S. (2004). *Carbon*, *42*, 3169; Jiang, J., Saito, R., Gruneis, A., Chou, S. G., Samsonidze, Ge. G., Jorio, A., Dresselhaus, G., & Dresselhaus, M. S. (2005). *Phys. Rev. B*, *71*, 045417.
[3] Dresselhaus, M. S., Dresselhaus, G., Saito, R., & Jorio, A. (2005). *Phys. Reports*, *409*, 47.
[4] Chou, S. G., Plentz Filho, F., Jiang, J., Saito, R., Nezich, D., Ribeiro, H. B., Jorio, A., Pimenta, M. A., Samsonidze, Ge. G., Santos, A. P., Zheng, M., Onoa, G. B., Semke, E. D., Dresselhaus, G., & Dresselhaus, M. S. (2005). *Phys. Rev. Lett.*, *94*, 127402.
[5] Samsonidze, Ge. G., Saito, R., Kobayashi, N., Gruneis, A., Jiang, J., Jorio, A., Chou, S. G., Dresselhaus, G., & Dresselhaus, M. S. (2004). *Appl. Phys. Lett.*, *85*, 5703.
[6] Gruneis, A. (2004). Ph. D. Thesis, *Tohoku University*, Sendai, Japan.
[7] Gruneis, A., Saito, R., Samsonidze, Ge. G., Kimura, T., Pimenta, M. A., Jorio, A., Souza Filho, A. G., Dresselhaus, G., & Dresselhaus, M. S. (2003). *Phys. Rev.*, *B 67*, 165402.
[8] Canccado, L. G., Pimenta, M. A., Jorio, A., Neves, R. A., Medeiros-Ribeiro, G., Enoki, T., Kobayashi, Y., Takai, K., Fukui, K., Dresselhaus, M. S., & Saito, R. (2004). *Phys. Rev. Lett.*, *93*, 047403.
[9] Jiang, J., Saito, R., Samsonidze, Ge. G., Chou, S. G., Jorio, A., Dresselhaus, G., & Dresselhaus, M. S. (2005). *Phys. Rev. B*, *72*, 235408.
[10] Saito, R., Jorio, A., Hafner, J., Lieber, C. M., Hunter, M., McClure, T., Dresselhaus, G., Dresselhaus, M. S. *et al*. (2001). *Phys. Rev. B, 63*, 085312.
[11] Yu, Z. & Brus, L. E. (2001). *J. Phys. Chem. B*, *105*, 6831.